Letter

Attosecond photoionization delays as time-domain photoelectron holography in polyatomic molecules

Ling-Hui Yao [1,2] Alexandra S. Landsman [3] Xu Wang [4] Liang-Wen Pi [1,*] and Yuxi Fu [1,†]

[1] *State Key Laboratory of Ultrafast Optical Science and Technology, Xi'an Institute of Optics and Precision Mechanics, Chinese Academy of Sciences, Xi'an 710119, China*

[2] *School of Future Technology, University of Chinese Academy of Sciences, Beijing 100049, China*

[3] *Department of Physics, The Ohio State University, Columbus, Ohio 43210, USA*

[4] *Graduate School, China Academy of Engineering Physics, Beijing 100193, China*

(Received 9 May 2026; accepted 14 July 2026; published 31 July 2026)

Attosecond photoionization time delays carry direct information about molecular structure, but isolating that structural contribution remains a central challenge in polyatomic systems. Here, we introduce a single-scattering framework that separates the ionization process into an iodine giant dipole resonance transition and subsequent electron propagation. Applied to iodopropane isomers, the method yields angle-resolved amplitudes, phases, and Wigner time delays, and shows that the delay is controlled by interference between direct and structurally scattered electron waves. We reproduce the experimentally observed isomer-dependent delay differences, showing that they originate from distinct geometric arrangements. Our results establish a form of attosecond electron holography in the time domain, identifying structural contributions to attosecond delays in complex molecules.

DOI: 10.1103/2f6k-vpl5

Introduction. To understand and control electron dynamics—central goals in physics, chemistry, and biology—it is crucial to probe these processes on their intrinsic timescales, which range from femtoseconds to attoseconds. Historically, direct observation of the time-dependent evolution of electron wave packets was hindered by the lack of sufficiently fast probes. Advances in ultrashort-pulse technology, particularly the development of attosecond pulses [1–7], now make it possible to pursue a central goal of ultrafast atomic, molecular, and optical physics: probing molecular structural evolution—especially real-time atomic motion—on attosecond timescales during transient electronic motion. At the same time, interference between direct and scattered electron wave packets underlies both ultrafast photoelectron diffraction [8–12] and strong-field photoelectron holography [13–15]. In the perturbative regime, photoelectron diffraction provides a direct probe of molecular structure through scattering from multiple atomic centers, whereas in strong-field holography the interference is shaped by laser-driven electron trajectories following tunneling ionization. Here, we extend these concepts to photoionization delay experiments, exploring attosecond electron holography in the time domain.

For an accurate description of electron dynamics, time delay is a quantity of central interest. Attosecond chronoscopy has revealed small but measurable delays in the photoemission process. In previous studies, attosecond photoemission delays have been measured mainly using two approaches: streaking experiments with isolated attosecond XUV pulses and reconstruction of attosecond beating by interference of two-photon transitions with attosecond pulse trains [16–18]. Key aspects of ionization time delays—including angular dependence, relativistic effects, and attochirp phenomena—have been systematically investigated using these methods [19–21]. Most previous studies of ionization time delays have focused on atomic targets, while only in recent years have experimental investigations been extended to molecules [22–24]. However, a clear physical interpretation for polyatomic molecules is still lacking. There are several reasons for this difficulty. First, closely spaced energy levels can produce spectral congestion, complicating the isolation of specific ionization channels [19,25]. Second, the ionization process generally consists of two conceptual steps: the initial ejection of the electron and its subsequent propagation through the molecular framework. Because these steps are difficult to disentangle, it is challenging to establish clear criteria for separating structural effects from the propagation of the photoelectron wave packet.

To address these challenges, we simulate attosecond ionization delays in iodopropane isomers through the I $4d \rightarrow \epsilon f$ giant dipole resonance (GDR). This choice offers two key advantages. First, the GDR is an inner-shell effect predominantly localized on the iodine atom [26–28]. Second, the outgoing f-wave dominates the iodine $4d$ giant-resonance region. This is supported by several connected observations. Calculations for Xe $4d$ photoionization show that the $4d \rightarrow \epsilon p$ contribution is much smaller than the $4d \rightarrow \epsilon f$

*Contact author: lwpi@opt.ac.cn

†Contact author: fuyuxi@opt.ac.cn

contribution, and iodine follows a similar $4d$ time-delay trend [29–31]. Iodine photoabsorption also shows a dominant $4d \rightarrow \epsilon f$ shape resonance, while CH_3I measurements show an atomiclike I $4d$ response over the energy range considered here [32–34]. Together, these results support using the dominant iodine-centered $4d \rightarrow \epsilon f$ launch to isolate structure-dependent delays from the propyl group [35].

The role of isomerism in molecular ionization time delays remains largely unexplored. Isomers provide an ideal platform for such investigations because they share the same chemical composition but differ in atomic arrangement. This contrast makes it possible to isolate the influence of molecular geometry on ionization dynamics.

Framework and results. Here, we briefly introduce the simulation based on a single-scattering model. Further details can be found in Refs. [9,36–38]. Unless otherwise specified, atomic units (a.u.) are used throughout.

An XUV photon ionizes an electron from a localized inner orbital. The emitted photoelectron then scatters off neighboring atoms, producing a diffraction-induced time delay that encodes the molecular structure [22,23,28,35]. This delay arises from the interference between direct and scattered electron waves. The structures of the iodopropane isomers are shown schematically in Fig. 1. In our analysis, the iodine atom is placed at the origin of the coordinate system. The three carbon atoms are labeled C1, C2, and C3 in order of increasing distance from the iodine atom. Structural parameters for the iodopropane isomers are taken from the PubChem database (CIDs: 6362 and 33643), which provides standardized structural data for chemical compounds [39,40]. To simplify the discussion, we define the molecular axis by the I–C3 bond in 1-iodopropane and by the I–C1 bond in 2-iodopropane. Because of isomerism, electrons emitted from the iodine atom encounter different propyl groups, leading to distinct Wigner time delays. Scattering from hydrogen atoms is neglected because its influence is substantially weaker than that of carbon. Over the photon-energy range considered here (60–200 eV), the elastic scattering cross section for hydrogen is approximately one order of magnitude smaller than that for carbon [41,42].

Assuming that linearly polarized XUV light along the z axis ejects an electron from a core orbital localized on the iodine atom, we adopt the spherical-wave approximation for the outgoing electron wave packet. In iodine, the GDR induces photoemission predominantly from the $4d$ orbital. The escaping wave packet therefore has a dominant f-wave character. The angular momentum quantum number for the emitted f wave is 3. In the compact notation used here, the total wave function in the far-field limit can be written as

$$\Psi(r,\theta,\phi,\Omega) \propto U_{\text{atom}}(r) \sum_m D^{3*}_{0,m}(\Omega)[Y_{3m}(\theta,\phi)+\Psi_{\text{pg}}(\theta,\phi)], \tag{1}$$

$$\Psi_{\text{pg}}(\theta,\phi) \approx \sum_i \frac{e^{ikR_i}}{R_i} Y_{3m}(\theta_i,\phi_i) f_i(\vartheta_i) e^{-i\boldsymbol{k}(\theta,\phi)\cdot\boldsymbol{R}_i}, \tag{2}$$

where $U_{\text{atom}}(r)$ is the far-field radial atomic wave function and is independent of the molecular structure. The orientational dependence is contained in the Wigner D-matrix $D^{3*}_{0,m}(\Omega)$, where Ω denotes the Euler angles. Here, 0 and m are the magnetic quantum numbers in the laboratory and molecular frames, respectively; we set the laboratory-frame projection to 0 and sum over m from -3 to 3. Within the brackets, $Y_{3m}(\theta,\phi)$ is the direct wave and $\Psi_{\text{pg}}(\theta,\phi)$ is the propyl-group contribution. In Eq. (2), R_i, θ_i, ϕ_i are the spherical coordinates of the ith scatterer relative to iodine, $\boldsymbol{k}$ is the final photoelectron momentum, and $f_i(\vartheta_i)$ is the elastic scattering amplitude [41] with scattering angle $\vartheta_i(\theta,\phi)$ between $\boldsymbol{R}_i$ and $\boldsymbol{k}$.

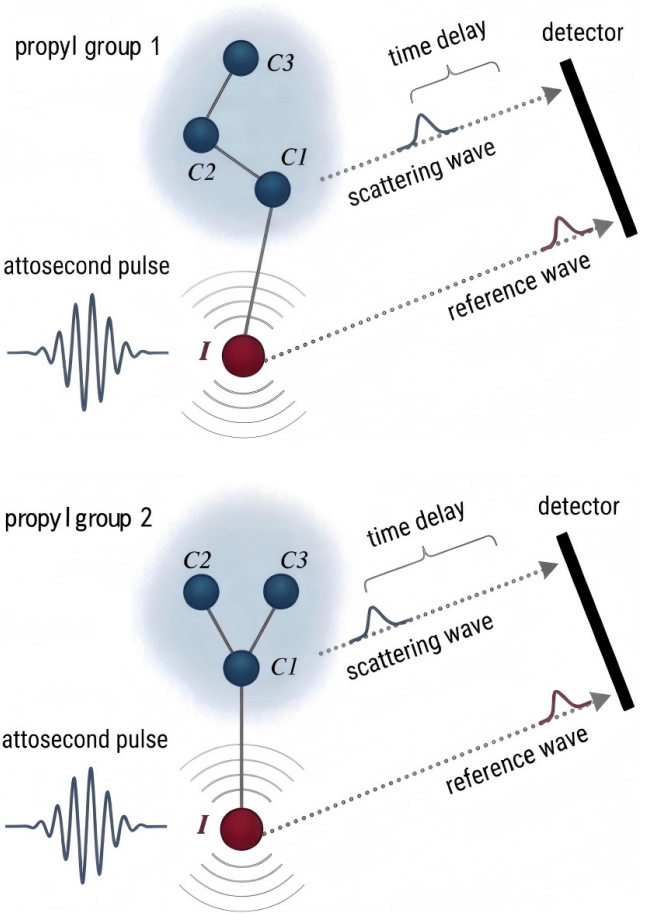

FIG. 1. Schematic illustration of the photoionization process in iodopropane isomers. An attosecond pulse triggers the initial ionization of the iodine atom, generating a reference wave. The emitted photoelectron then scatters off the distinct propyl-group arrangements shown in the upper and lower panels, producing a scattering wave. The interference between the reference and scattering waves encodes the structural differences into a measurable time delay.

In this compact picture, the iodine-centered GDR launch acts as the reference emission, while Ψ_{pg} collects the additional amplitudes and phases generated when the outgoing electron encounters the surrounding carbon framework. This separation allows us to attribute changes in the delay primarily to molecular structure rather than to the initial atomic excitation step.

Equation (1) is therefore a single-channel representation of the dominant $4d \rightarrow \epsilon f$ launch. The weaker $4d \rightarrow \epsilon p$ channel is not included. This omitted transition would launch an outgoing p-wave component. Its inclusion would add direct p-f interference, interference between the direct waves and their scattered counterparts, and interference between

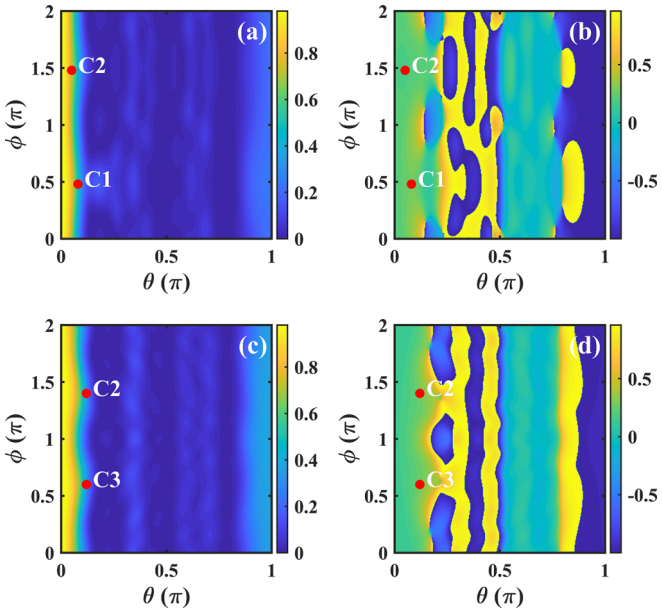

FIG. 2. (a) Amplitude and (b) phase distribution of 1-iodo propane. (c) Amplitude and (d) phase distribution of 2-iodopropane.

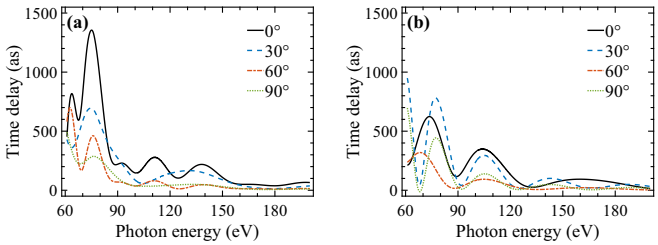

FIG. 3. Results computed in the GDR photon-energy range of about 60–200 eV. The black, blue, red, and green curves correspond to orientation angles β of 0°, 30°, 60°, and 90°, respectively. (a) Computed $\tau_{pg}(E, \Omega)$ for 1-iodopropane. (b) Computed $\tau_{pg}(E, \Omega)$ for 2-iodopropane.

scattered p- and f-wave components. These terms can modify calculated amplitudes, cross sections, photoelectron angular distributions, and local phase maps, especially where the f-wave amplitude is small. In the present work, we neglect them in order to isolate the leading structure-dependent scattering phase generated by the propyl group.

Notably, our calculations include only single-scattering events and neglect higher-order scattering contributions. Although trajectories involving multiple scatterings before detection are physically possible, this approximation is justified for two reasons. In the intermediate-to-high energy regime, the probability of multiple scattering is orders of magnitude smaller than that of single scattering. Moreover, previous theoretical benchmarks show that the differences in computed time delays between single- and multiple-scattering formalisms are negligible [43]. For the present iodopropane isomers, the dominant structural phase is therefore expected to be set by the first encounter of the outgoing electron with the propyl group, which is precisely the contribution needed to resolve the isomer dependence.

First, we present the calculated amplitudes and phases for the two iodopropane isomers at an emitted-electron energy of 105 eV, consistent with Ref. [35], with the molecular axis aligned along the polarization direction. Figure 2 shows the corresponding amplitude and phase maps. The relevant spherical coordinates (θ_i, ϕ_i) are marked; C3 in 1-iodopropane and C1 in 2-iodopropane are not labeled because they lie on the z axis ($\theta = 0$), for which the azimuthal angle ϕ is arbitrary. Each amplitude map is normalized to its own maximum. The more symmetric propyl group in 2-iodopropane produces clear interference fringes reminiscent of a double-slit pattern, whereas the amplitude and phase distributions of 1-iodopropane are less symmetric. As illustrated in Fig. 2, the scattering phases are more sensitive to the molecular structure than the transition amplitudes. Because photoionization time delays are directly derived from these phases, this enhanced sensitivity allows our time-domain approach to resolve structural details that are typically inaccessible in conventional electron diffraction and holography experiments.

These calculations show that the fixed-orientation amplitude and phase fingerprints are set directly by the propyl-group geometry. This confirms that the observed interference is generated by molecular structure and provides the basis for the time-delay analysis below.

Building on the calculated amplitudes and phases, we determine the Wigner time delay. At a sufficiently large radial distance, the outgoing wave reaches its asymptotic form. We then write the energy-dependent outgoing wave as $\Psi(E, \theta, \phi, \Omega)$ and define the phase as

$$\varphi(E, \theta, \phi, \Omega) = \arg\left[\Psi(E, \theta, \phi, \Omega)\right]. \tag{3}$$

The angle-resolved Wigner time delay is the energy derivative of this phase [22,27,44,45]:

$$\tau_w(E, \theta, \phi, \Omega) = \frac{d\varphi(E, \theta, \phi, \Omega)}{dE} = \tau_{\text{atom}}(E, \theta, \phi, \Omega) + \tau_{\text{pg}}(E, \theta, \phi, \Omega), \tag{4}$$

where τ_{pg} denotes the delay contribution generated by propagation and scattering in the propyl-group environment, whereas τ_{atom} provides the iodine-centered atomic reference.

In principle, the orientation angle Ω between the molecular axis (defined as the I–C3 axis for 1-iodopropane and the I–C1 axis for 2-iodopropane) and the polarization direction of the incident light can be varied continuously. To examine its influence, we fix the photon polarization along the z axis and systematically rotate the molecular axis toward the y axis within the y–z plane. In this configuration, the orientation angle Ω corresponds to $(0, \beta, 0)$ in the Euler-angle representation. Varying the orientation angle strongly affects both the amplitude and phase distributions. Using the resulting amplitude and phase information, we calculate the theoretical propyl-group contribution $\tau_{pg}(E, \Omega)$ for the two isomers. These computations cover photon energies from 60 to 200 eV. The results for $\beta = 0°, 30°, 60°$, and $90°$ are shown in Fig. 3.

Within this energy range, our calculations predict positive time delays that gradually decrease with increasing photon energy and eventually approach zero, consistent with previous studies [22,27]. This behavior arises because higher

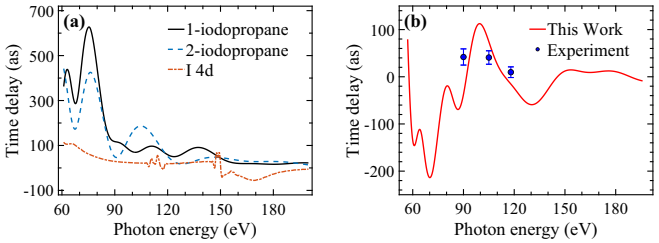

FIG. 4. Orientation-averaged observables. (a) Orientation-averaged time delays. The black and blue curves represent the orientation-averaged propyl-group time delays for the two isomers of iodopropane. The red curve represents the atomic ionization time delay of iodine. (b) The red curve represents the theoretical calculation of $\tau_{2\text{-iodo}}(E) - \tau_{1\text{-iodo}}(E)$. The blue symbols with vertical error bars represent the experimental isomer delay difference taken from Ref. [35]; the error bars are estimated from the reported uncertainties of the individual isomer delays.

photon energies impart more kinetic energy to electrons emitted through inner-shell ionization. Faster, higher-energy electrons spend less time in the molecular environment and are therefore less affected by its potential. Conversely, lower-energy electrons are more strongly influenced by the molecule, leading to larger delay differences. Our calculations also show that the time delays are most sensitive to structural changes at small orientation angles (black and blue lines). This sensitivity arises because iodine 4*d* electrons are emitted primarily along the z axis, i.e., along the polarization direction. Aligning the molecular axis with this direction places the carbon atoms directly in the densest part of the electron cloud, generating a strong diffraction pattern that clearly encodes the molecular structure. At larger orientation angles, this overlap is reduced, so the structural contrast is progressively washed out even though the overall positive delay trend remains.

To compare with experiment, we extend our analysis to the full three-dimensional space by statistically sampling 10 000 random orientations. In experiments, when the molecules are not fixed in space, one must average over all possible molecular orientations. When all orientations are equally probable, we obtain

$$\tau_w(E) = \frac{\int_\Omega \tau_w(E,\Omega) d\Omega}{\int_\Omega d\Omega}. \tag{5}$$

This gives the orientation-averaged time delay as a function of energy. Details of the calculation of τ_{atom} can be found in Refs. [26,27]. The iodine atomic delay is isotropic and unchanged by orientation averaging. Figure 4(a) shows the orientation-averaged propyl-group delays for the two isomers, together with the common iodine reference [27]. Figure 4(b) compares $\tau_{2\text{-iodo}}(E) - \tau_{1\text{-iodo}}(E)$ with experiment [35].

The isomer delay difference arises from different propyl-group geometries. Our model qualitatively reproduces the experimental trend in the 90–120 eV range. The positive delay difference survives orientation averaging. This shows that the structural signal is robust, not a fixed-orientation artifact.

Quantitative discrepancies nevertheless remain. The theory overestimates the delay magnitude and misses the oscillation amplitudes at 90 and 120 eV. This likely reflects our use of scattering form factors from isolated carbon atoms, rather than a correlated molecular environment [46]. Even so, the model correctly predicts a positive isomer-dependent delay difference after orientation averaging.

The present model also omits relativistic fine structure, electron correlation, and exchange [30,47–49]. These effects can shift absolute delays and modify angular distributions. Because both isomers share the same iodine-centered ionization step, these iodine-core effects are expected to contribute largely as a common component, although a full multichannel treatment could also modify the detailed angular and phase dependence. The leading contrast remains the structure-dependent scattering phase set by the propyl-group geometry. Future work could include these effects more fully and combine molecular-continuum methods with *ab initio* molecular dynamics [50].

Conclusions. In summary, we have developed a theoretical framework that isolates structural contributions to attosecond ionization delays in iodopropane isomers. The key mechanism is interference between direct and scattered photoelectron wave packets, which converts differences in the propyl-group geometry into measurable delay shifts. Our calculations show that even electrically neutral atoms can make an essential contribution to the scattering-induced delay.

After full orientation averaging, the isomer-dependent delay difference remains positive and agrees qualitatively with experiment. This shows that the structural signal is robust and survives beyond fixed-orientation conditions. More broadly, by accessing structural information through the spectral phase rather than traditional intensity-based observables, our results provide a useful framework for interpreting attosecond time delays. This establishes a form of attosecond electron holography in the time domain, enabling structural sensitivity in complex polyatomic molecules beyond the reach of existing approaches.

Acknowledgments. L.-H.Y. and L.-W.P. acknowledge support from the National Natural Science Foundation of China (12374322) and the Chinese Academy of Sciences (YSBR-115). A.S.L. acknowledges DOE, Atomic, Molecular and Optical Sciences Program under Award No. DE-SC0022093. X.W. acknowledges support from the National Natural Science Foundation of China (12474484 and 12088101). Y.F. acknowledges support from the Chinese Academy of Sciences (YSBR-091 and 29J22-083-III) and the Natural Science Basic Research Program of Shaanxi (2019JCW-03). This work was supported by the computing resources provided by the Computing Center in Xi'an.

Data availability. There are no publicly available research data or software supporting this manuscript. Requests for further information or data should be sent to the authors.

[1] M. Hentschel, R. Kienberger, C. Spielmann, G. A. Reider, N. Milosevic, T. Brabec, P. Corkum, U. Heinzmann, M. Drescher, and F. Krausz, Attosecond metrology, Nature (London) **414**, 509 (2001).

[2] P. M. Paul, E. S. Toma, P. Breger, G. Mullot, F. Augé, P. Balcou, H. G. Muller, and P. Agostini, Observation of a train of attosecond pulses from high harmonic generation, Science **292**, 1689 (2001).

[3] G. Sansone, L. Poletto, and M. Nisoli, Isolated single-cycle attosecond pulses, Science **314**, 443 (2006).

[4] E. Goulielmakis, Z.-H. Loh, A. Wirth, R. Santra, N. Rohringer, V. S. Yakovlev, S. Zherebtsov, T. Pfeifer, A. M. Azzeer, M. F. Kling, S. R. Leone, and F. Krausz, Single-cycle nonlinear optics, Science **320**, 1614 (2008).

[5] K. Zhao, Q. Zhang, M. Chini, Y. Wu, X. Wang, and Z. Chang, Tailoring a 67 attosecond pulse through advantageous phase-mismatch, Opt. Lett. **37**, 3891 (2012).

[6] T. Gaumnitz, A. Jain, Y. Pertot, M. Huppert, I. Jordan, F. Ardana-Lamas, and H. J. Wörner, Streaking of 43-attosecond soft-X-ray pulses generated by a passively CEP-stable mid-infrared driver, Opt. Express **25**, 27506 (2017).

[7] J. Li, X. Ren, Y. Yin, K. Zhao, A. Chew, Y. Cheng, E. Cunningham, Y. Wang, S. Hu, Y. Wu, M. Chini, and Z. Chang, 53-attosecond X-ray pulses reach the carbon K-edge, Nat. Commun. **8**, 186 (2017).

[8] M. Meckel *et al.*, Laser-induced electron tunneling and diffraction, Science **320**, 1478 (2008).

[9] F. Krasniqi, B. Najjari, L. Strüder, D. Rolles, A. Voitkiv, and J. Ullrich, Imaging molecules from within: Ultrafast angström-scale structure determination of molecules via photoelectron holography using free-electron lasers, Phys. Rev. A **81**, 033411 (2010).

[10] C. I. Blaga, J. Xu, A. D. DiChiara, E. Sistrunk, K. Zhang, P. Agostini, T. A. Miller, L. F. DiMauro, and C. D. Lin, Imaging ultrafast molecular dynamics with laser-induced electron diffraction, Nature (London) **483**, 194 (2012).

[11] R. Boll, J. Mikosch, A. S. Tremsin, T. Osipov, B. Murphy, N. Berrah, C. Bostedt, J. D. Bozek, P. H. Bucksbaum, M. Fehrenbach, M. Guhr, D. Heinz, L. J. Frasinski, J. Krzywinski, M.-F. Lin, S. Mukamel, J. C. Robinson, T. J. A. Wolf, Z.-D. Zhang, and D. Rolles, Imaging molecular structure through femtosecond photoelectron diffraction on aligned and oriented gas-phase molecules, Faraday Discuss. **171**, 57 (2014).

[12] D. Rolles, M. S. Schöffler, H. Adaniya, T. Osipov, B. Murphy, J. D. Bozek, C. Bostedt, A. C. Cassidy, T. J. A. Wolf, L. Fang, M. Hoener, O. Gessner, A. Belkacem, and N. Berrah, Femtosecond x-ray photoelectron diffraction on gas-phase dibromobenzene molecules, J. Phys. B: At. Mol. Opt. Phys. **47**, 124035 (2014).

[13] M. Meckel, A. Staudte, S. Patchkovskii, D. M. Villeneuve, P. B. Corkum, R. Dörner, and M. Spanner, Signatures of the continuum electron phase in molecular strong-field photoelectron holography, Nat. Phys. **10**, 594 (2014).

[14] G. Porat *et al.*, Attosecond time-resolved photoelectron holography, Nat. Commun. **9**, 2805 (2018).

[15] T. Khurelbaatar, J. Heo, S. Yu, X. Lai, X. Liu, and D. E. Kim, Strong-field photoelectron holography in the subcycle limit, Light: Sci. Appl. **13**, 108 (2024).

[16] M. Schultze *et al.*, Delay in photoemission, Science **328**, 1658 (2010).

[17] K. Klünder, J. M. Dahlström, M. Gisselbrecht, T. Fordell, M. Swoboda, D. Guénot, P. Johnsson, J. Caillat, J. Mauritsson, A. Maquet, R. Taıeb, and A. L'Huillier, Probing single-photon ionization on the attosecond time scale, Phys. Rev. Lett. **106**, 143002 (2011).

[18] M. Ossiander *et al.*, Absolute timing of the photoelectric effect, Nature (London) **561**, 374 (2018).

[19] R. Pazourek, S. Nagele, and J. Burgdörfer, Attosecond chronoscopy of photoemission, Rev. Mod. Phys. **87**, 765 (2015).

[20] F. Calegari, G. Sansone, S. Stagira, C. Vozzi, and M. Nisoli, Advances in attosecond science, J. Phys. B: At. Mol. Opt. Phys. **49**, 062001 (2016).

[21] F. Krausz, The birth of attosecond physics and its coming of age, Phys. Scr. **91**, 063011 (2016).

[22] M. Huppert, I. Jordan, D. Baykusheva, A. von Conta, and H. J. Wörner, Attosecond delays in molecular photoionization, Phys. Rev. Lett. **117**, 093001 (2016).

[23] J. Vos, L. Cattaneo, S. Patchkovskii, T. Zimmermann, C. Cirelli, M. Lucchini, A. Kheifets, A. S. Landsman, and U. Keller, Orientation-dependent stereo Wigner time delay and electron localization in a small molecule, Science **360**, 1326 (2018).

[24] A. Kamalov, A. L. Wang, P. H. Bucksbaum, D. J. Haxton, and J. P. Cryan, Electron correlation effects in attosecond photoionization of CO_2, Phys. Rev. A **102**, 023118 (2020).

[25] Z. Tao, C. Chen, T. Szilvási, M. Keller, M. Mavrikakis, H. Kapteyn, and M. Murnane, Direct time-domain observation of attosecond final-state lifetimes in photoemission from solids, Science **353**, 62 (2016).

[26] H. P. Kelly and Z. Altun, Atomic many body theory of giant resonances, in *Giant Resonances in Atoms, Molecules, and Solids*, edited by J. P. Connerade, J. M. Esteva, and R. C. Karnatak (Springer, Boston, MA, 1987), pp. 71–89.

[27] L.-W. Pi and A. Landsman, Attosecond time delay in photoionization of noble-gas and halogen atoms, Appl. Sci. **8**, 322 (2018).

[28] S. Biswas *et al.*, Probing molecular environment through photoemission delays, Nat. Phys. **16**, 778 (2020).

[29] L.-W. Pi and A. F. Starace, Potential-barrier effects in three-photon-ionization processes, Phys. Rev. A **90**, 023403 (2014).

[30] S. Zhong *et al.*, Attosecond electron-spin dynamics in Xe 4*d* photoionization, Nat. Commun. **11**, 5042 (2020).

[31] B. Grafstrom and A. S. Landsman, Attosecond time delay trends across the isoelectronic noble gas sequence, Atoms **11**, 84 (2023).

[32] G. O' Sullivan, The absorption spectrum of CH_3I in the extreme VUV, J. Phys. B: At. Mol. Phys. **15**, L327 (1982).

[33] G. O'Sullivan, C. McGuinness, J. T. Costello, E. T. Kennedy, and B. Weinmann, Trends in 4*d*-subshell photoabsorption along the iodine isonuclear sequence: I, I^+, and I^{2+}, Phys. Rev. A **53**, 3211 (1996).

[34] D. W. Lindle, P. H. Kobrin, C. M. Truesdale, T. A. Ferrett, P. A. Heimann, H. G. Kerkhoff, U. Becker, and D. A. Shirley, Inner-shell photoemission from the iodine atom in CH_3I, Phys. Rev. A **30**, 239 (1984).

[35] C. A. Schröder *et al.*, Photoemission chronoscopy of the iodoalkanes, Phys. Rev. A **112**, L051104 (2025).

[36] S. X.-L. Sun, A. P. Kaduwela, A. X. Gray, and C. S. Fadley, Progress toward time-resolved molecular imaging: A theoretical study of optimal parameters in static photoelectron holography, Phys. Rev. A **89**, 053415 (2014).

[37] X. Wang, A.-T. Le, C. Yu, R. R. Lucchese, and C. D. Lin, Retrieving transient conformational molecular structure

information from inner-shell photoionization of laser-aligned molecules, Sci. Rep. **6**, 23655 (2016).

[38] C. Yu and X. Wang, Improved molecular structure retrieval method for photoelectron holography, Phys. Rev. A **100**, 063422 (2019).

[39] PubChem, 2-Iodopropane, CID 6362, https://pubchem.ncbi.nlm.nih.gov/compound/6362.

[40] PubChem, 1-Iodopropane, CID 33643, https://pubchem.ncbi.nlm.nih.gov/compound/33643.

[41] F. Salvat, A. Jablonski, and C. J. Powell, Elsepa—Dirac partial-wave calculation of elastic scattering of electrons and positrons by atoms, positive ions and molecules, Comput. Phys. Commun. **165**, 157 (2005).

[42] A. Jablonski, F. Salvat, and C. J. Powell, *NIST Electron Elastic-Scattering Cross-Section Database—Version 4.0* (National Institute of Standards and Technology, Gaithersburg, MD, 2016).

[43] Y. Tamura, K. Yamazaki, K. Ueda, and K. Hatada, A multiple scattering theoretical approach to time delay in high energy core-level photoemission of heteronuclear diatomic molecules, J. Phys. B: At. Mol. Opt. Phys. **55**, 10LT01 (2022).

[44] E. P. Wigner, Lower limit for the energy derivative of the scattering phase shift, Phys. Rev. **98**, 145 (1955).

[45] F. T. Smith, Lifetime matrix in collision theory, Phys. Rev. **118**, 349 (1960).

[46] M. Li *et al.*, Photoionization time delays probe electron correlations, Phys. Rev. Lett. **135**, 183202 (2025).

[47] F. Brauße *et al.*, Time-resolved inner-shell photoelectron spectroscopy: From a bound molecule to an isolated atom, Phys. Rev. A **97**, 043429 (2018).

[48] T. Marx and S. I. Bokarev, A frequency-domain approach to molecular photoionization via driven Schrödinger equation, J. Chem. Phys. **162**, 184109 (2025).

[49] M. E. Riley and D. G. Truhlar, Approximations for the exchange potential in electron scattering, J. Chem. Phys. **63**, 2182 (1975).

[50] S. Severino *et al.*, Attosecond core-level absorption spectroscopy reveals the electronic and nuclear dynamics of molecular ring opening, Nat. Photon. **18**, 731 (2024).